Physiological Reports

Open Access

Physiological Reports ISSN 2051-817X

ORIGINAL RESEARCH

The vortex formation time to diastolic function relation: assessment of pseudonormalized versus normal filling

Erina Ghosh[1] & Sándor J. Kovács[1,2]

1 Department of Biomedical Engineering, School of Engineering and Applied Science, Washington University in St Louis, St. Louis, Missouri
2 Cardiovascular Biophysics Laboratory, Cardiovascular Division, Department of Internal Medicine, School of Medicine, Washington University in St Louis, St. Louis, Missouri

Keywords
Diastolic function, tissue Doppler imaging, transmitral flow, vortex formation.

Correspondence
Sándor J. Kovács, Cardiovascular Biophysics Laboratory, Washington University Medical Center, 660 South Euclid Ave, Box 8086, St. Louis, MO 63110.
Tel: (314)-362-8901
Fax: (314)-362-8957
E-mail: sjk@wuphys.wustl.edu

Funding Information
This work was supported in part by the Alan A. and Edith L. Wolff Charitable Trust (St. Louis, MO) and the Barnes-Jewish Hospital Foundation. E. G. is a recipient of a Heartland Affiliate predoctoral fellowship award from the American Heart Association (11PRE4950009).

Received: 11 October 2013; Revised: 30 October 2013; Accepted: 1 November 2013

doi: 10.1002/phy2.170

Physiol Rep, 1 (6), 2013, e00170, doi: 10.1002/phy2.170

Abstract

In early diastole, the suction pump feature of the left ventricle opens the mitral valve and aspirates atrial blood. The ventricle fills via a blunt profiled cylindrical jet of blood that forms an asymmetric toroidal vortex ring inside the ventricle whose growth has been quantified by the standard (dimensionless) expression for vortex formation time, $VFT_{standard}$ = {transmitral velocity time integral}/{mitral orifice diameter}. It can differentiate between hearts having distinguishable early transmitral (Doppler *E*-wave) filling patterns. An alternative validated expression, $VFT_{kinematic}$ reexpresses $VFT_{standard}$ by incorporating left heart, near "constant-volume pump" physiology thereby revealing $VFT_{kinematic}$'s explicit dependence on maximum rate of longitudinal chamber expansion (E'). In this work, we show that $VFT_{kinematic}$ can differentiate between hearts having indistinguishable *E*-wave patterns, such as pseudonormal (PN; $0.75 < E/A < 1.5$ and $E/E' > 8$) versus normal. Thirteen age-matched normal and 12 PN data sets (738 total cardiac cycles), all having normal LVEF, were selected from our Cardiovascular Biophysics Laboratory database. Doppler *E*-, lateral annular E'-waves, and *M*-mode data (mitral leaflet separation, chamber dimension) was used to compute $VFT_{standard}$ and $VFT_{kinematic}$. $VFT_{standard}$ did not differentiate between groups (normal [3.58 ± 1.06] vs. PN [4.18 ± 0.79], $P = 0.13$). In comparison, $VFT_{kinematic}$ for normal (3.15 ± 1.28) versus PN (4.75 ± 1.35) yielded $P = 0.006$. Hence, the applicability of $VFT_{kinematic}$ for diastolic function quantitation has been broadened to include analysis of PN filling patterns in age-matched groups.

Introduction

The ability to quantify diastolic function (DF) quantitatively is crucial in order to properly diagnose heart failure with preserved ejection fraction (HFpEF) or diastolic heart failure (DHF) (Zile and Brutsaert 2002; Gheorghiade and Pang 2009) and to assess the success of therapy. The preferred noninvasive method for DF assessment is Doppler echocardiography and various Doppler indexes are used to quantify DF (Klein and Garcia 2008; Nagueh et al. 2009). Most of these indexes are empiric (based on Doppler echocardiographic waveform features rather than on mechanisms) or correlation based, irrespective of causal relations. Hence, these indexes cannot provide mechanistic insight into the physiology of DF.

A mechanism-based approach for DF quantitation is available and is provided by the parametrized diastolic filling (PDF) formalism (Kovács et al. 1987). Because the heart is a mechanical oscillator, the formalism treats mechanical suction initiated early rapid (Doppler *E*-wave) filling in analogy to the recoil from rest, of a previously displaced, damped simple harmonic oscillator. Model

predicted fit to the clinical *E*-wave is excellent and the fitting process specifies three parameters: k, the stiffness constant; c, the viscoelastic damping/relaxation constant; and x_o, the volumetric preload. The PDF formalism has been validated in a broad range of normal and pathophysiologic settings (in humans and animals). The PDF parameters and indexes derived from them have been rigorously shown to have direct clinical relevance (Dent et al. 2001; Lisauskas et al. 2001a,b; Riordan and Kovács 2006; Shmuylovich and Kovács 2006). The PDF formalism has been automated (Hall and Kovács 1994; Hall et al. 1998) and solves the "inverse problem of diastole" (Hall and Kovács 1993) by providing a unique set of PDF parameters for each analyzed *E*-wave.

An alternate approach for DF characterization utilizes fluid mechanics. The left ventricle (LV) fills by aspirating atrial blood which forms an asymmetric toroidal (doughnut-shaped) vortex as it curls around the mitral leaflet tips (Hong et al. 2008). The vortex ring expands as the ventricle fills and the outer boundary of the vortex rinses the highly trabeculated endocardium preventing thrombus formation while concomitantly facilitating mitral leaflet coaptation during diastasis (Ghosh and Kovács 2011). The pattern of flow and vortex formation is affected by cardiac dysfunction and has been previously characterized via echocardiography using vortex formation time (VFT).

Gharib et al. (2006) used Doppler *E*-wave data to calculate $VFT_{standard}$ in subjects with normal LVEF and normal *E*-wave patterns and subjects with dilated cardiomyopathy and abnormal *E*-wave patterns. They found that subjects with normal *E*-wave patterns had a normal range of values (3.5–5.5), whereas subjects with dilated cardiomyopathy had lower $VFT_{standard}$.

We have previously derived and validated a complementary method of calculating VFT ($VFT_{kinematic}$) (Ghosh et al. 2009, 2010) involving the PDF formalism (Kovács et al. 1987) (See Appendix A for details). Our derivation made use of the near constant-volume physiologic attribute of the left heart (Bowman and Kovács 2003) that provides the algebraic relationship between effective mitral orifice area (diameter) and longitudinal annular tissue motion (E'). Our results demonstrated very good correlation between $VFT_{kinematic}$ and $(E/E')^{3/2}$, an established echocardiographic index of DF (Nagueh et al. 1997; Ghosh et al. 2010).

In this work, we test the hypothesis that $VFT_{kinematic}$ can distinguish between normal and diastolic dysfunction (pseudonormal [PN] filling) states where both groups are age matched and have indistinguishable, normal *E*-wave patterns. To test our hypothesis we analyzed 738 beats and computed $VFT_{kinematic}$ and $VFT_{standard}$ in 25 subjects and performed an intergroup comparison.

Methods

Subject selection criteria

Echocardiographic data from 25 subjects were selected from the Cardiovascular Biophysics Laboratory database. Prior to data acquisition, subjects provided signed, informed consent for participation in accordance with the Institutional Review Board (Human Research Protection Office) at Washington University School of Medicine. The inclusion criteria were as follows: normal sinus rhythm, absence of valvular abnormalities and the absence of wall-motion abnormalities or bundle branch block on the ECG, normal LVEF, normal valvular function, and clearly identifiable *E*- and A-waves and E'-waves. In addition, all subjects also had Doppler *M*-mode images of the mitral leaflet motion recorded in the parasternal view.

We dichotomized subjects into normal and PN groups, according to American Society of Echocardiography (ASE) (Nagueh et al. 2009) criteria. In both groups $0.75 < E/A < 1.5$, in the normal group, lateral E'_{peak} velocity was >10 cm/sec and $E/E' < 8$ and in the PN group, lateral E'_{peak} velocity was reduced (<10 cm/sec) resulting in $E/E' > 8$. All subjects (both groups) had normal LV ejection fraction (>50%) and either normal coronary anatomy or insignificant (<50%) coronary artery narrowing. Because diastolic filling patterns (Klein et al. 1994) and $VFT_{standard}$ depend on age (Gharib et al. 2006), we specifically age matched the groups so that age could not be a distinguishing metric.

Doppler echocardiography

Our data acquisition method has been previously detailed (Shmuylovich and Kovács 2006; Ghosh et al. 2010). Briefly, echocardiography was performed in accordance with published ASE criteria (Nagueh et al. 2009). Immediately before catheterization, patients were imaged in a supine position using a Philips iE33 system (Best, the Netherlands). Two-dimensional images in apical two- and four-chamber views were obtained with the sample volume gated at 1.5–2.5 mm directed between the tips of the mitral valve leaflets and orthogonal to the mitral valve plane (to minimize misalignment effects). The wall filter was set at 125 or 250 Hz, the baseline adjusted to take advantage of the full height of the display and the velocity scale adjusted to exploit the dynamic range of the output without aliasing. The four-chamber view was used to record Doppler *E*-waves and tissue Doppler E'-waves (Fig. 1A and C). For E'-wave recording the lateral aspect of mitral annulus was selected because recent studies have shown that in patients with normal ejection fraction, lateral E' has the best correlation with LV filling pressures

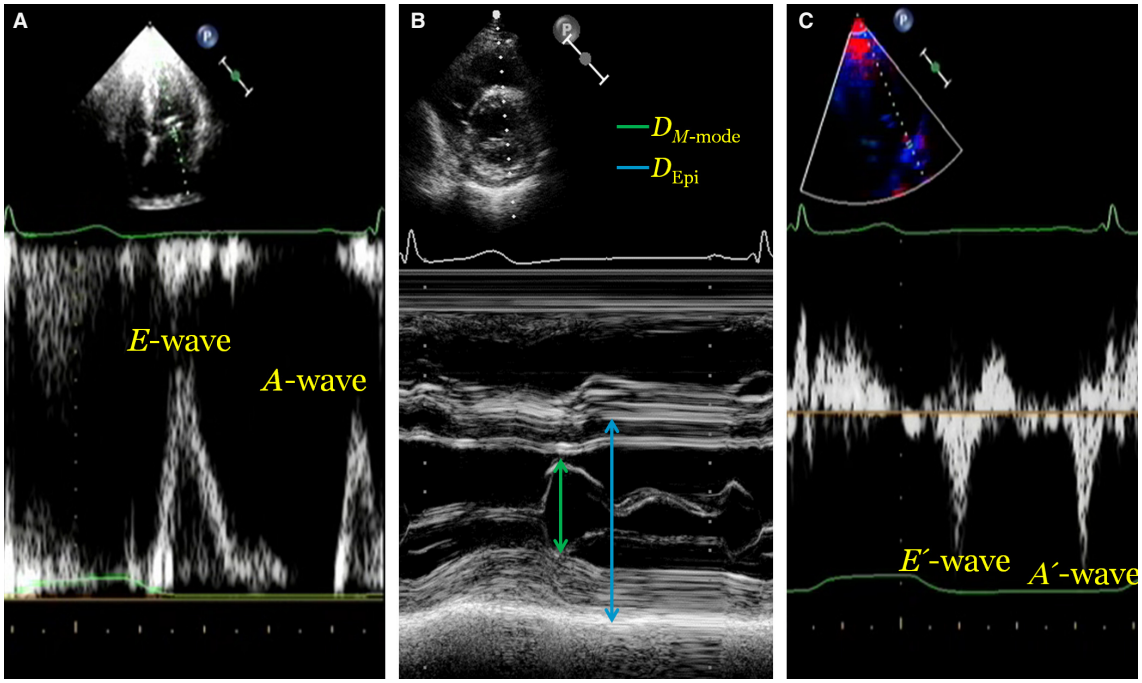

Figure 1. (A) Typical Doppler transmitral flow image showing one cardiac cycle with Doppler *E*- and *A*-wave marked. (B) Typical parasternal *M*-mode image with peak mitral leaflet separation ($D_{M\text{-mode}}$) in green and epicardial diameter (D_{epi}) in blue. (C) Typical tissue Doppler, lateral mitral annulus motion image with Doppler *E*′- and *A*′-wave marked. See text for details.

and invasive indices of LV stiffness (Kasner et al. 2007). Doppler *M*-mode images recorded in the parasternal short-axis view (as shown in Fig. 1B) were used to determine mitral leaflet separation for effective orifice diameter computation following the European Association of Echocardiography (EAE)/ASE guidelines (Baumgartner et al. 2009).

Doppler data analysis

The transmitral Doppler waveforms and the tissue Doppler *E*′-waves were analyzed using two methods: (1) the conventional method and (2) the PDF formalism, using best *E*-wave contour fit criteria in computing the PDF (x_o, c, k) parameters. In the conventional method, the *E*-wave is approximated as a triangle such that its height is peak velocity (E_{peak}) and its base is the duration (E_{dur}). The same method is used to analyze Doppler *E*′-wave and determine E'_{peak} and E'_{dur}.

The second method of *E*-wave analysis employs the PDF formalism (Kovács et al. 1987) which solves the "inverse-problem of diastole" (Hall and Kovács 1993) (See Appendix A). The method of PDF parameter determination has been automated and detailed previously (Hall et al. 1998; Riordan and Kovács 2006) and has an interobserver variability of 8% (Boskovski et al. 2008).

The peak mitral leaflet separation was calculated from *M*-mode images in accordance with (Gharib et al. 2006). The epicardial dimension D_{epi} was also measured from the same *M*-mode image using the method described by Foppa et al. (2005). Figure 1B shows a typical *M*-mode image with the diameters marked.

Calculation of VFT

The method of calculating $VFT_{kinematic}$ and $VFT_{standard}$ has been previously detailed (Ghosh et al. 2010). Briefly, $VFT_{standard}$ is defined as the *E*-wave area (triangle method) divided by the maximum mitral leaflet separation.

$$VFT_{standard} = \frac{E_{peak} \times E_{dur}}{2 \times D_{M-mode}} \quad (1)$$

Using equation (1), $VFT_{standard}$ is calculated for each *E*-wave using the needed parameters determined from the conventional method described in the previous section. The diameter is measured from parasternal *M*-mode image as shown in Fig. 1B. We have previously shown (Ghosh et al. 2010) that the *E*-wave area calculated via the triangle method is equivalent to *E*-wave area calculated by integrating the PDF fit curvilinear contour of the *E*-wave.

$VFT_{kinematic}$ also uses the same *E*-wave area divided by the orifice diameter expression. However, *E*-wave area is calculated using the PDF formalism derived curvilinear fit and the flow orifice diameter is derived by incorporating the near constant volume attribute of the left heart (Bowman and Kovács 2003; Ghosh et al. 2010). The previously derived and validated expression for $VFT_{kinematic}$ is as follows:

$$VFT_{kinematic} = \frac{x_o(1+\exp(-c\pi/2\omega))}{D_{epi}\sqrt{E'/E}} \quad (2)$$

where D_{epi} is a constant, the epicardial diameter measured from *M*-mode images (blue line in Fig. 1B), *c*, and x_o are PDF parameters, and ω is the angular frequency of a full oscillation, the initial half of which corresponds to the *E*-wave. These are obtained by analyzing the Doppler *E*-wave (Fig. 1A) using the PDF formalism. In the denominator, E'_{peak} and E_{peak} are obtained as in the conventional analysis.

Numerical methods and statistical analyses

Images were recorded in DICOM format and converted into bitmap images using a custom MATLAB program (MATLAB 6.0 MathWorks, Natick, MA). Another MATLAB script was written to compute the conventional triangle fit to Doppler *E*- and *E*′-waves. The PDF parameters were computed using an error-minimizing algorithm (Levenberg–Marquardt algorithm) as detailed briefly in Appendix (A) and fully in previous work (Ghosh et al. 2010). $VFT_{kinematic}$ and $VFT_{standard}$ values were computed for each beat using a custom MATLAB program. $VFT_{standard}$ was calculated for each *E*-wave using equation 1 and $VFT_{kinematic}$ was calculated by matching *E*- and *E*′-waves with close R-R intervals (<10 msec difference). For each subject, the values of VFT were averaged for all the beats. Student's *t*-test (two tailed) was used to determine the significance of difference between the two groups. $P < 0.05$ was considered statistically significant. Regression analysis was performed to validate the relationship between both the VFTs and $(E/E')^{3/2}$. The average values were correlated and Pearson's product moment correlation coefficient (R^2) for each linear regression was determined.

Results

A total of 738 beats from 25 subjects were analyzed (average 30 beats/subject). Table 1 provides group demographics involving 12 men and 13 women. Nine men and four women were in the normal group and three men and nine women were in the PN group. The groups were age matched (normal = 59 years, range: 49–73 years and PN = 61 years, range: 47–78 years, $P = 0.59$). Body surface area and weight of the two groups were not significantly different. The left ventricular end diastolic pressure (LVEDP) of 14 mmHg for normal and 16 mmHg for PN ($P = 0.12$) did not differ between groups. The EF of all subjects was normal. Although normal, the EF of the PN group was higher (74%) than the EF of the normal group (67%). The mean resting HR was slightly higher in the PN group (71 bpm) than normal (61 bpm).

Echo parameters: Table 2 gives the group average values of echocardiographic parameters and PDF parameters. There was no statistical difference between Doppler *E*-wave parameters (conventional and PDF) between the two groups. The E_{peak} was 70 cm/sec for normal and was

Table 1. Subject demographics showing data for the two groups and the *P*-value (Column 4).

Parameter	Normal (n = 13)	PN (n = 12)	*P*-value
Age (years)	59 (9)	61 (12)	NS 0.59
Gender	9M, 4F	3M, 9F	
Weight (lbs)	177 (28)	189 (54)	NS 0.49
Height (cm)	173 (8)	160 (14)	0.014
BSA (m^2)	1.95 (0.2)	1.96 (0.3)	NS 0.96
EDP (mm Hg)	14 (3)	16 (4)	NS 0.12
Ejection Fraction (%)	67 (9)	74 (7)	0.03
Mean HR (bpm)	61 (8)	71 (13)	0.04
Beats Analyzed	26 (18)	33 (21)	NS 0.41

$P < 0.05$ is considered statistically significant. The standard deviation values are in parenthesis.

Table 2. *E*- and *E*′-wave parameters.

Parameters	Normal (n = 13)	PN (n = 12)	*P*-values
E_{peak} (cm/sec)	70 (16)	72 (13)	NS 0.76
E_{dur} (msec)	294 (26)	299 (31)	NS 0.66
DT (msec)	200 (28)	203 (32)	NS 0.81
A_{peak} (cm/sec)	55 (11)	82 (16)	<0.001
E/*A*	1.3 (0.3)	0.9 (0.2)	<0.001
E'_{peak} (cm/sec)	14 (5)	7 (1)	<0.001
E/*E*′	5.3 (1.4)	10.4 (2.0)	<0.001
VTI (cm)	10 (3)	11 (2)	NS 0.67
PDF parameters			
k	263 (53)	254 (53)	NS 0.68
c	23 (6)	25 (7)	NS 0.43
x_o	9.2 (2.1)	10.3 (2.3)	NS 0.21

The mean values for each group are listed along with *P*-value. $P < 0.05$ denotes statistical significance. Parentheses denote standard deviations. VTI, velocity time integral; PDF, parametrized diastolic filling.

72 cm/sec for PN. The E_{dur}, DT, and the velocity time integral (VTI) were not different between the groups. The A_{peak} velocity was higher in PN group (82 cm/sec) than normal (55 cm/sec). Although E/A was statistically different between the two groups, the value for both the groups was in the normal range (0.75–1.5) for the age range (Nagueh et al. 2009). In accordance with convention for PN patterns, E'_{peak} velocity was significantly lower in the PN group (normal = 14 cm/sec vs. PN = 7 cm/sec, $P < 0.001$), however E'_{dur} was not different. In accordance with PN pattern criteria E/E' was significantly higher than control (normal = 5.3 vs. PN = 10.7, $P < 0.001$).

VFT values: The mean $VFT_{kinematic}$ for the normal group was 3.15 and for the PN group it was 4.75. $VFT_{standard}$ for the normal group was 3.59 and for PN it was 4.18. The differences in $VFT_{kinematic}$ were statistically significant ($P = 0.006$), whereas the differences in $VFT_{standard}$ were not ($P = 0.13$). This is shown in Figure 2. Table 3 lists the value of $VFT_{kinematic}$ and $VFT_{standard}$ for all subjects.

Discussion

Vortex ring formation in the LV manifests nature's solution to the "atrium to ventricle mass transfer problem," while maintaining efficient filling by helping to preserve the momentum of blood flow and by optimally aligning streamlines toward the outflow tract (Gharib et al. 1998; Mohseni and Gharib 1998; Krueger and Gharib 2003; Pedrizzetti and Domechini 2005; Pasipoularides 2010; Töger et al. 2012). The fluid mechanics of vortex formation has been extensively studied and adapted to quantify LV filling dynamics (Kheradvar et al. 2007). Studying the physiology of filling through VFT provides a novel way to assess DF. We previously derived and validated an alternate expression for VFT which includes explicit E/E' dependence (Ghosh et al. 2010). In this study, we build on that foundation by extending the physiologic realm of VFT applicability by testing the ability of the alternate VFT expression to differentiate between age-matched controls and subjects with PN filling (characterized by essentially indistinguishable E-wave patterns). Our goal in this study was to demonstrate the advantage of using a physiology based expression of VFT to quantify diastolic filling, rather than enhancing the understanding of LV vortex dynamics.

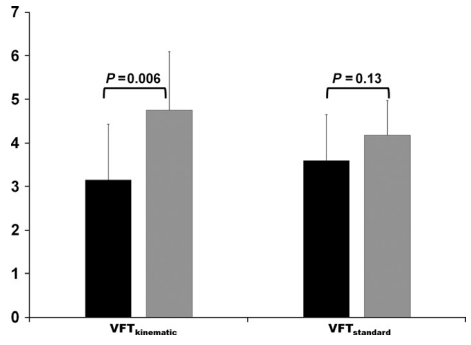

Figure 2. Comparing $VFT_{kinematic}$ and $VFT_{standard}$ in the normal and PN groups. The bars on the left compare the value of $VFT_{kinematic}$ in normal (dark gray) and PN (light gray) subjects. The bars on the right show the same comparison for $VFT_{standard}$ values. The error bars represent the standard deviation for the four values. The P-values of the intergroup comparison for each VFT value is given. See text for details. VFT, vortex formation time; PN, pseudonormal.

Previous studies

To facilitate clinical application Gharib et al. (2006) proposed a simplified definition for VFT described above (eq. 1). Using this expression they showed that $VFT_{standard}$ had an optimal range of values. Other studies (Lee et al. 2007; Jiamsripong et al. 2009a,b; Kheradvar et al. 2012) have also shown that $VFT_{standard}$ can differentiate between normal E-wave patterns and selected pathologic E-wave patterns.

$VFT_{standard}$ uses only Doppler E-wave features and mitral orifice diameter at a single time point during filling. However, there is a causal relationship between chamber (motion) kinematics and fluid (motion), hence VFT can be shown to depend on the kinematic attributes of the LV (Ghosh et al. 2009, 2010). Vortex formation is affected by how the LV accommodates volume, which includes longitudinal (characterized by the tissue Doppler E'-wave) and radial filling volume components. By incorporating near constant volume physiology, $VFT_{kinematic}$ explicitly takes into account longitudinal motion at the level of the annulus. As a consequence, we previously (Ghosh et al. 2010, Appendix B) demonstrated that in an idealized (cylindrical) LV aspirating essentially constant E-wave volumes (in reality <10% variation among subjects), VFT is proportional to $(E/E')^{3/2}$. We achieved a significant correlation of $VFT_{kinematic}$ versus $(E/E')^{3/2}$ while $VFT_{standard}$ failed to achieve a significant correlation versus $(E/E')^{3/2}$.

Recently, Kheradvar et al. (2012) calculated $VFT_{standard}$ in four groups of subjects grouped according to E-wave patterns: normal, impaired relaxation, PN relaxation, and restrictive filling. They showed that $VFT_{standard}$ was significantly different among the four groups, demonstrating the ability of $VFT_{standard}$ to correlate with altered transmitral filling patterns associated with increasing dysfunction. However, the results were confounded by age, since the

Table 3. $VFT_{kinematic}$ and $VFT_{standard}$ for all 25 subjects with associated component values.

Subject No.	$VFT_{kinematic}$	$VFT_{standard}$	Epicardial diameter (cm)	Maximum leaflet Separation (cm)	E_{peak} (m/sec)	E'_{peak} (m/sec)	E/E'
1	2.6	3.3	7.0	2.9	0.57	0.15	3.7
2	1.5	2.2	10	3.6	0.50	0.11	4.5
3	1.8	2.0	7.8	3.4	0.52	0.11	4.7
4	1.9	3.3	7.9	2.6	0.53	0.10	5.1
5	2.2	3.7	7.8	2.4	0.65	0.13	5.1
6	3.0	3.1	6.5	2.8	0.66	0.12	5.6
7	4.6	4.5	6.1	2.8	0.90	0.16	5.7
8	4.1	3.9	7.3	3.6	0.86	0.12	7.1
9	5.8	6.3	6.4	2.5	1.02	0.14	7.1
10	3.3	3.8	6.5	2.7	0.70	0.13	5.3
11	3.9	3.8	6.1	2.5	0.71	0.14	5.5
12	2.2	3.2	6.1	3.1	0.67	0.29	2.3
13	4.1	3.5	7.6	3.3	0.84	0.11	7.7
14	3.3	3.8	8.7	2.5	0.69	0.08	8.6
15	4.5	4.2	6.4	2.3	0.62	0.07	8.6
16	1.9	2.8	11	3.0	0.55	0.07	8.5
17	4.5	3.9	5.9	2.4	0.74	0.08	9.2
18	6.7	5.2	6.4	2.5	0.76	0.07	11.4
19	6.7	5.7	6.8	2.4	0.92	0.07	12.7
20	6.0	4.6	6.9	2.5	0.87	0.07	13.3
21	4.5	3.4	6.3	2.5	0.61	0.05	13.6
22	4.9	3.9	6.6	2.7	0.68	0.06	11.8
23	5.3	4.3	6.5	2.7	0.81	0.09	9.1
24	4.6	4.7	9.2	3.0	0.89	0.09	9.3
25	4.0	3.7	6.9	2.5	0.52	0.06	9.1

Subjects 1–13 are the normal group. Subjects 14–25 are the PN group. VFT, vortex formation time; PN, pseudonormal.

age of the normal subject group was less than half of the ages of the other three groups (Normals = 28 years vs. DD = 63 years). Previous work by Gharib et al. (2006) (Fig. 3 of referenced paper) has shown that $VFT_{standard}$ decreases substantially with age. In light of this dependence of $VFT_{standard}$ on age, the reported differences in $VFT_{standard}$ in (Kheradvar et al. 2012) are confounded by age.

Identifying PN filling

In moderate DD, characterized by PN filling, the transmitral *E*- and *A*-wave shapes have the same characteristics as *E*- and *A*-waves in normal subjects. An example is shown in Figure 3 which shows *E*-waves from two subjects. The *E*-waves are indistinguishable using conventional metrics such as peak velocity, duration, VTI, and E/A (Table 4). However, they have different peak E'. $VFT_{standard}$ cannot distinguish between these two subjects because it depends only on *E*-wave features. However, $VFT_{kinematic}$ can differentiate between them because it incorporates E'. The PN pattern of DD has impaired longitudinal motion, elevated LAP while maintaining a normal *E*-wave shape.

For this study, we selected subjects whose echo data satisfy the established criteria for the PN pattern by having *E*-waves similar to the normal group, normal LV function (EF > 50%) but impaired longitudinal (E') motion. The PN group had $E'_{peak} < 10$ cm/sec and $E/E' > 8$. Previous studies (Nagueh et al. 1997; Mohseni and Gharib 1998) have used E/E' to estimate filling pressures and to assess DF in subjects with normal EF. We used their cutoff value of 8 to dichotomize into PN versus normal groups. In addition, to ensure that the difference in the E/E' ratio is not due to reduced E_{peak} velocity, we required lateral $E'_{peak} < 10$ cm/sec for the PN group. Previous studies have shown (Klein et al. 1994; Hill and Palma 2005) that for the age range in this study, normal E'_{peak} velocities have a mean value of ~11 cm/sec. As DF becomes impaired with age (Klein et al. 1994; Ommen and Nishimura 2003; Hill and Palma 2005; Nagueh et al. 2009), we age matched the groups. The Doppler *E*-wave attributes in both of the groups studied were similar (Table 2). The two groups differed in the Doppler E'_{peak} representing the peak longitudinal volume accommodation rate.

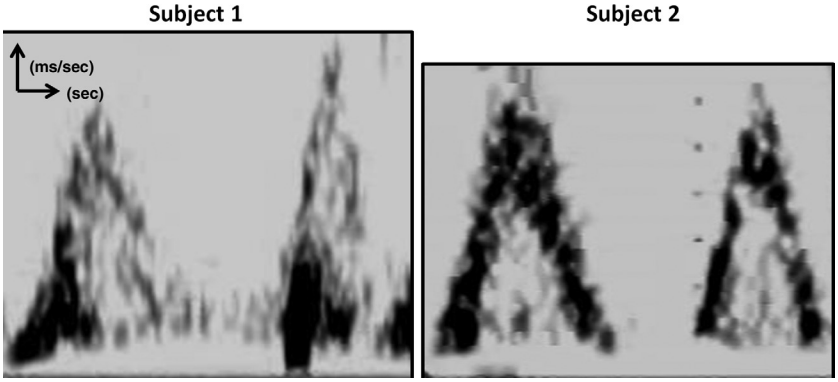

Figure 3. Comparing the ability of $VFT_{kinematic}$ and $VFT_{standard}$ to differentiate between two similar Doppler *E*-waves. The *E*-wave image on the left (marked Subject 1) is from Subject 5 (Table 3; normal group). The image on the right (marked Subject 2) is from Subject 17 (PN group). $VFT_{standard}$ can not differentiate between these two waves while $VFT_{kinematic}$ can differentiate between them. See text and Table 4 for details. VFT, vortex formation time.

Table 4. Features of two Doppler *E*-waves shown in Figure 3 with associated VFT values.

Parameter	Subject 1	Subject 2
E_{peak} (cm/sec)	60	60
E_{dur} (msec)	217	217
HR (bpm)	68	61
E'_{peak} (cm/sec)	12	6.6
$VFT_{standard}$ (dimensionless)	2.71	2.69
$VFT_{kinematic}$ (dimensionless)	1.75	3.16

The two *E*-waves are indistinguishable in terms of mean E_{peak}, E_{dur}, and *E/A*. HR and $VFT_{standard}$ values.

In our previous work, we derived and demonstrated the relationship between VFT and $(E/E')^{3/2}$ (Appendix B, Ghosh et al. 2010). Using the constant volume attribute (Bowman and Kovács 2003) we demonstrated that for the same *E*-wave volume, VFT is inversely proportional to D^3, where D is effective orifice diameter. Since D is proportional to $\sqrt{(E'/E)}$, VFT is proportional to $(E/E')^{3/2}$. As $VFT_{kinematic}$ incorporates the constant volume attribute, it provides a better correlation with $(E/E')^{3/2}$ than $VFT_{standard}$. Figure 4 compares $VFT_{kinematic}$ and $VFT_{standard}$ to $(E/E')^{3/2}$. Although the relationship between VFT and $(E/E')^{3/2}$ is based on approximations (assuming that the LV is a cylinder with no epicardial radial expansion and *E*-wave volumes among subjects remain essentially constant), $VFT_{kinematic}$ had a good correlation with $(E/E')^{3/2}$ ($R^2 = 0.55$). In most of the normal subjects, (open circles; 9 of 13) $VFT_{kinematic} < 4$ and in most PN subjects (10 of 12), $VFT_{kinematic} > 4$ (Fig 4A). $VFT_{standard}$, however, had a poor correlation with $(E/E')^{3/2}$ (Fig. 4B). There is no clear value of $VFT_{standard}$ which can differentiate between the groups. This is restated in Table 3, which lists the mean values of $VFT_{kinematic}$ and $VFT_{standard}$ for all subjects. Hence, $VFT_{kinematic}$ not only correlates better with *E/E′*, an established DF index (Nagueh et al. 1997) but is also able to better dichotomize between groups. Our study builds upon our previous work and expands the applicability of $VFT_{kinematic}$.

Physiological and clinical significance

Traditionally, VFT has been computed in vitro using a piston-cylinder arrangement where the fluid exited the nozzle and formed vortices in a larger (essentially unbounded) space (Dabiri and Gharib 2005; Kheradvar and Gharib 2008). In the LV, the fluid (blood) is aspirated through the mitral orifice into a smaller (bounded) space (LV chamber) where expanding vortex ring dimension is comparable to expanding chamber dimension (Töger et al. 2012). In this scenario, the rate of chamber expansion plays an important role in vortex formation by actually generating the space for the vortex ring to expand into while providing the energy to generate the flow (since early transmitral filling is powered by the LV chamber recoil/suction). Optimal vortex formation occurs when vortex ring size and growth is synchronized with chamber size and chamber expansion (Kheradvar et al. 2007; Kheradvar and Gharib 2008). A mismatch between these two dynamic (tissue motion and fluid motion) attributes, as seen in enlarged chambers with a low LVEF, results in suboptimal vortex formation, indicative of less efficient utilization of recoil energy and associated mass transfer (Töger et al. 2012). When the rate of chamber expansion is slower than vortex ring growth, (as in an enlarged chamber) the kinetic energy of blood is lost and fluid momentum is not directed toward the outflow track

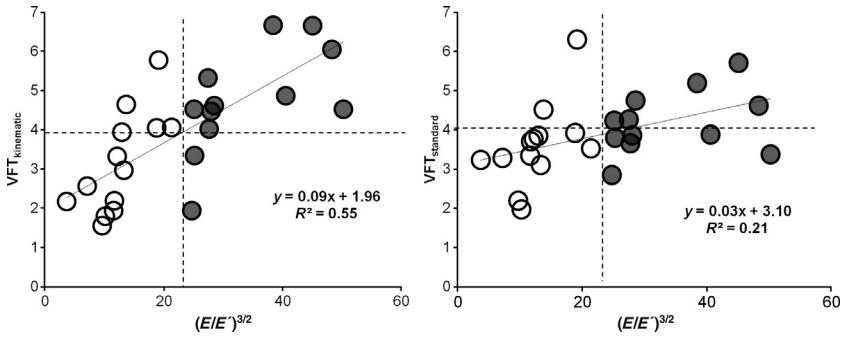

Figure 4. Comparing $VFT_{kinematic}$ and $VFT_{standard}$ to $E/E'^{3/2}$. Open circles represent subjects in the normal group and closed subjects represent subjects in the PN group. (A) Correlation between $VFT_{kinematic}$ and $E/E'^{3/2}$. The two ratios are well correlated ($R^2 = 0.55$) and nine of 13 subjects in the normal group have $VFT_{kinematic} < 4$. Eleven of 13 subjects in PN group have $VFT_{kinematic} > 4$. (B) Correlation between $VFT_{standard}$ and $E/E'^{3/2}$. The two ratios are not well correlated and no clear cutoff value for $VFT_{standard}$ exists. Ten of 12 normal subjects had $VFT_{standard} < 4$ and six of 12 PN subjects had $VFT_{standard} > 4$. See text for details. VFT, vortex formation time; PN, pseudonormal.

for optimal subsequent ejection. This has been shown by Carlhäll and Bolger (2010) who found that in normal hearts most of the ejected blood volume entered the LV in the same beat, whereas in subjects with moderate heart failure, the volume of blood entering and exiting the LV in the same beat is decreased. Consequently, the LV has to provide the energy to eject the stagnant blood thereby making the filling and ejection process less efficient. Tissue Doppler E' velocity has been shown to be reduced in DD. A slower longitudinal chamber expansion rate corresponding to lower E'_{peak} or a higher E/E' ratio is a correlate of higher filling pressures (Nagueh et al. 1997; Lisauskas et al. 2001b). In terms of energetics, this means that the ventricle does more work to fill to the same volume.

Thus, by explicitly including chamber expansion (E'), $VFT_{kinematic}$ includes the relation of filling physiology to fluid mechanics. The original expression for $VFT = v*t/D = L/D$, where v is flow velocity and t is time of flow duration, facilitates inclusion of the near constant-volume attribute of the left heart. Specifically, near constant volume means that left atrial and ventricular volumes reciprocate as a result of ascent and descent of the mitral annulus and LV wall thickening and thinning throughout the cardiac cycle, hence the LA–LV summed total (epicardial) volume is essentially constant. This defines the algebraic (volume conserving) relation among LV wall thinning, transmitral flow (E-wave), mitral annular velocity (E'-wave) flow orifice diameter (D), and constant epicardial dimension.

Another issue that affects the calculation of both $VFT_{kinematic}$ and $VFT_{standard}$ is the question of relative versus absolute velocity. In deriving VFT and expressing it as $v*t/D = L/D$, the implicit assumption is that the flow velocity is measured relative to a stationary orifice. In the heart, however, the ultrasonic transducer defines the origin of the coordinate system relative to which transmitral flow (E-wave) is measured. Whereas the blood enters the ventricle at the velocity of the E-wave, the orifice (mitral annulus and valve) is moving in the opposite direction (relative to the transducer) at the velocity of the E'-wave. Hence, relative to the orifice itself, the blood is moving at velocity $E + E'$. This has the effect of increasing the VTI relative to the original value by about 10% for normals and by about 5% for PNs (because E' VTI is statistically significantly lower in the PN group). If we recalculate group differences correcting for the motion of the annulus (i.e. using $E + E'$) for VTI rather than just E, our results remain unaltered, we again find that statistically significant difference between $VFT_{kinematic}$ $P = 0.011$ versus $VFT_{standard}$ $P = 0.26$ is maintained. Recall, prior to the $E + E'$ "correction" the differences in $VFT_{kinematic}$ were $P = 0.006$ whereas for $VFT_{standard}$ it was $P = 0.13$.

DHF or HFpEF is present in ~50% of patients admitted to hospitals with heart failure. The mortality rate of HFpEF is slightly lower than the subjects with reduced ejection fraction (Bhatia et al. 2006; Owan et al. 2006). Echocardiography is the preferred method for noninvasive diagnosis and grading of HF (Nagueh et al. 2009). Previous studies have shown (Møller et al. 2000) that in patients after a myocardial infarction, PN filling was an independent predictor of mortality. Subjects with PN filling had higher mortality than patients with normal filling or impaired relaxation. A specific therapeutic approach for selective treatment of HFpEF still eludes us (Schwartzenberg et al. 2012). Hence, the availability of indexes that incorporate fluid mechanics attributes of filling and can differentiate PN from normal filling is of value.

Although the fact that the PN and normal groups in this sample can be easily differentiated using conventional

metrics (E', EF, A_{peak}) may be initially viewed as a limitation to ultimate clinical utility, the fact that $VFT_{kinematic}$ is derived from basic principles of fluid mechanics, and incorporates near constant volume (Bowman and Kovács 2003) and suction pump physiology of the LV while providing explicit time-dependent expressions for its components enhances its ultimate value in merging fluid mechanics–based analysis of DF.

Currently, fluid streamline imaging is in its infancy, but the rapid advancement of noninvasive imaging technology will lead to streamline information application in multiple modalities such as echo, MRI, and CT (recall the advances in echo from 1*D* (*M*-mode) to 2*D* to Doppler, to color-Doppler to 3*D*) (Sengupta et al. 2012). The characterization of the relation between VFT and physiology will become increasingly important and will likely lead to understanding of new relationships between flow and chamber function. Currently, this form of *VFT is* a crude (lumped parameter) metric of the (global) wall motion (DF) to streamline generation relation. When viewed in this context, our work is the first step in incorporating the physiology and merging the technology of streamline imaging and characterization and global DF. We anticipate full, high spatial, and temporal resolution, 3D streamline information availability as the technology advances.

Limitations

Limitations arise from the definition (eqs. 1 and 2) and the echocardiographic data used to calculate them. The various assumptions and limitations in calculating $VFT_{kinematic}$ and $VFT_{standard}$ have been discussed previously (Ghosh et al. 2010). The peak mitral leaflet separation is calculated from *M*-mode images in parasternal short-axis view that can be affected by a poor acoustic window, transducer position, and the angulation relative to LV long axis. To mitigate these effects we made multiple measurements of the diameter whenever possible and averaged over measured values. We also measure the diameter from one-dimensional *M*-mode measurement which might result in error if the orifice is not round or if the measurements were not made at the center of the valve plane. Because this is an accepted limitation of *M*-mode imaging, we took care to calculate VFT using the method previously used in (Gharib et al. 2006; Ghosh et al. 2010).

The calculation of $VFT_{kinematic}$ should use simultaneous *E*- and E'-waves. Accordingly we matched *E*- and E'-waves by selecting beats with R-R intervals within $\pm$10 msec of each other. All subjects had a diastatic interval, hence the minor R-R differences affect only diastasis duration.

The number of subjects in the groups is constrained by the number of subjects in the Cardiovascular Biophysics Laboratory database who satisfy the inclusion criteria. The large number of beats analyzed (738) mitigates this limitation to an acceptable degree and provides adequate power for our statistics-based conclusions. However, clinical use awaits studies having a larger sample size. We have specifically chosen groups with normal ejection fraction and clinically indistinguishable *E*-waves to demonstrate the advantage of $VFT_{kinematic}$ over $VFT_{standard}$ to detect differences. Gharib et al. (2006) and Kheradvar et al. (2012) have shown that VFT in subjects with reduced ejection fraction is different from subjects with a normal ejection fraction.

Another potential limitation of the study is gender distribution. While the overall number of men and women studied was nearly equal, they were unequally divided into the two groups. The normal group had nine men of 13, whereas the PN group had nine women of 12. The gender-based differences in Doppler echocardiographic indexes are well documented (Sadaniantz et al. 1997; Bella et al. 2002). Claessens et al. (2011) computed conventional and PDF *E*-wave parameters (x_o, c, and k) and found that in 1606 age-matched subjects (862 females/744 males) the PDF parameters x_o, c, and k were significantly lower in males as compared to females. Other studies (Park et al. 2007) have reported no significant gender-based differences in E/A, *E*-wave DT, and E/E' (lateral or septal). However, the effect of gender on VFT has not been studied. In this study, we computed the gender-based group average for $VFT_{kinematic}$ and $VFT_{standard}$ and found that these values were not statistically different between men and women. Hence, in our study, gender did not affect the difference in $VFT_{kinematic}$ between normal and PN groups. However, to reliably assess gender-related issues larger groups will need to be studied. Nonetheless since HFpEF is more prevalent in women (Bhatia et al. 2006), the PN subset in our study approximates that population.

Conclusion

VFT defined as $VFT_{standard}$ = {*E*-wave VTI}/{mitral orifice diameter} has been shown to differentiate between diastolic dysfunction groups defined by distinguishable *E*-wave patterns and decreasing LVEF. To extend the clinical realm of VFT applicability, we tested the hypothesis that VFT can also differentiate between age-matched groups having PN patterns versus age-matched controls, with normal EF and indistinguishable *E*-waves. We compared $VFT_{kinematic}$ and $VFT_{standard}$ and found that $VFT_{kinematic}$ could differentiate between groups. Because $VFT_{kinematic}$ incorporates E' it expands the clinical realm of VFT applicability.

Acknowledgments

The assistance of Peggy Brown in expert echocardiographic data acquisition and the assistance of the staff of the Barnes-Jewish Hospital Cardiovascular Procedure Center at Washington University Medical Center are gratefully acknowledged.

Conflict of Interest

None declared.

References

Baumgartner, H., J. Hung, J. Bermejo, J. B. Chambers, A. Evangelista, B. P. Griffin, et al. 2009. Echocardiographic assessment of valve stenosis: EAE/ASE recommendations for clinical practice. J. Am. Soc. Echocardiogr. 22:1–23.

Bella, J. N., V. Palmieri, D. W. Kitzman, J. E. Liu, A. Oberman, S. C. Hunt, et al. 2002. Gender differences in diastolic function in hypertension (the HyperGEN study). Am. J. Cardiol. 89:1052–1056.

Bhatia, R. S., J. V. Tu, D. S. Lee, P. C. Austin, J. Fang, A. Haouzi, et al. 2006. Outcome of heart failure with preserved ejection fraction in a population-based study. N. Eng. J. Med. 355:260–269.

Boskovski, M. T., L. Shmuylovich, and S. J. Kovács. 2008. Transmitral flow velocity- contour variation after premature ventricular contractions: A novel test of the load-independent index of diastolic filling. Ultrasound Med. Biol. 34:1901–1908.

Bowman, A. W., and S. J. Kovács. 2003. Assessment and consequences of the constant-volume attribute of the four-chambered heart. Am. J. Physiol. 285:H2027–H2033.

Carlhäll, C. J., and A. Bolger. 2010. Passing strange: flow in the failing ventricle. Circ. Heart Fail. 3:326–331.

Claessens, T., M. W. Raja, A. Pironet, J. Chirinos, T. Desaive, E. Rietzschel, et al. 2011. The parametrized diastolic filling formalism: application in the Asklepios population. Proc. Assoc. Mech. Eng. 2011 Summer Bioengineering Conference (SBC-2011:53375). Farmington, PA, 22 June 2011.

Dabiri, J. O., and M. Gharib. 2005. The role of optimal vortex formation in biological fluid transport. Proc. Biol. Sci. 272:1557–1560.

Dent, C. L., A. W. Bowman, M. J. Scott, J. S. Allen, J. B. Lisauskas, M. Janif, et al. 2001. Echocardiographic characterization of fundamental mechanisms of abnormal diastolic filling in diabetic rats with a parameterized diastolic filling formalism. J. Am. Soc. Echocardiogr. 14:1166–1172.

Foppa, M., B. B. Duncan, and L. E. P. Rohde. 2005. Echocardiography-based left ventricular mass estimation. How should we define hypertrophy? Cardiovasc. Ultrasound. 3:17.

Gharib, M., E. Rambod, and K. Shariff. 1998. A universal time-scale of vortex formation time. J. Fluid Mech. 360:121–140.

Gharib, M., E. Rambod, A. Kheradvar, D. J. Sahn, and J. O. Dabiri. 2006. Optimal vortex formation as an index of cardiac health. Proc. Natl Acad. Sci. USA 103:6305–6308.

Gheorghidae, M., and P. S. Pang. 2009. Acute heart failure syndromes. J. Am. Coll. Cardiol. 53:557–573.

Ghosh, E., and S. J. Kovács. 2011. *E*-wave associated vortex formation facilitates diastatic mitral leaflet coaptation. J. Am. Coll. Cardiol. 57:E663.

Ghosh, E., L. Shmuylovich, and S. J. Kovács. 2009. Determination of early diastolic LV vortex formation time (T*) via the PDF formalism: a kinematic model of filling. Conf. Proc. IEEE Eng. Med. Biol. Soc. 2009:2883–2886.

Ghosh, E., L. Shmuylovich, and S. J. Kovács. 2010. Derivation of the fluid mechanics to left ventricular early, rapid filling relation, with in-vivo validation. J. Appl. Physiol. 109:1812–1819.

Hall, A. F., and S. J. Kovács Jr. 1993. Processing parameter effects on the robustness of the solution to the "Inverse Problem" of diastole from Doppler echocardiographic data. Conf. Proc. IEEE Eng. Med. Biol. Soc. Pp. I385–I387.

Hall, A. F., and S. J. Kovács. 1994. Automated method for characterization of diastolic transmitral Doppler velocity contours: Early rapid filling. Ultrasound Med. Biol. 20:107–116.

Hall, A. F., S. P. Nudelman, and S. J. Kovács Jr. 1998. Evaluation of model-based processing algorithms for averaged transmitral spectral Doppler images. Ultrasound Med. Biol. 24:55–66.

Hill, J. C., and R. A. Palma. 2005. Doppler tissue imaging for the assessment of left ventricular diastolic function: a systemic approach for the sonographer. J. Am. Soc. Echocardiogr. 18:80–90.

Hong, G. R., G. Pedrizzetti, G. Tonti, P. Li, Z. Wei, J. K. Kim, et al. 2008. Characterization and quantification of vortex flow in the human left ventricle by contrast echocardiography using vector particle image velocimetry. JACC Cardiovasc. Imaging 1:705–717.

Jiamsripong, P., A. M. Calleja, M. S. Alharthi, E. J. Cho, E. M. McMahon, J. J. Heys, et al. 2009a. Increase in late diastolic filling force is associated with impaired transmitral flow efficiency in acute moderate elevation left ventricular afterload. J. Ultrasound Med. 28:175–182.

Jiamsripong, P., A. M. Calleja, M. S. Alharthi, M. Dzsinich, E. M. McMahon, J. J. Heys, et al. 2009b. Impact of acute moderate elevation in left ventricular afterload on diastolic transmitral flow efficiency: analysis by vortex formation time. J. Am. Soc. Echocardiogr. 22:427–431.

Kasner, M., D. Westermann, P. Steendijk, R. Gaub, U. Wilkenshoff, K. Weitmann, et al. 2007. Utility of Doppler echocardiography and tissue Doppler imaging in the estimation of diastolic function in heart failure with normal

ejection fraction: a comparative Doppler-conductance catheterization study. Circulation 116:637–647.

Kheradvar, A., and M. Gharib. 2008. On mitral valve dynamics and its connection to early diastolic flow. Ann. Biomed. Eng. 37:1–13.

Kheradvar, A., M. Milano, and M. Gharib. 2007. Correlation between vortex ring formation and mitral annulus dynamics during ventricular rapid filling. ASAIO J. 53:8–16.

Kheradvar, A., R. Assadi, A. Falahatpisheh, and P. P. Sengupta. 2012. Assessment of transmitral vortex formation in patients in diastolic dysfunction. J. Am. Soc. Echocardiogr. 25:220–227.

Klein, A. L., and M. J. Garcia. 2008. Diastology: clinical approach to diastolic heart failure, 1st ed. Saunders, Philadelphia, PA.

Klein, A. L., D. J. Burstow, A. J. Tajik, P. K. Zachariah, K. R. Bailey, and J. B. Seward. 1994. Effects of age on left ventricular dimensions and filling dynamics in 117 normal persons. Mayo Clin. Proc. 69:212–224.

Kovács, S. J., B. Barzilai, and J. E. Pérez. 1987. Evaluation of diastolic function with Doppler echocardiography: the PDF formalism. Am. J. Physiol. 87:H178–H187.

Kovács, S. J., Jr, J. S. Meisner, and E. L. Yellin. 2000. Modeling of diastole. Cardiol. Clin. 18:459–487.

Krueger, P., and M. Gharib. 2003. The significance of vortex ring formation to the impulse and thrust of a starting jet. Phys. Fluids 15:1271–1281.

Lee, L. C., Y. L. Tan, H. C. Tan, A. R. Omar, P. Chai, T. C. Yeo, et al. 2007. Abstract 3289: vortex formation index in heart failure: novel non-invasive assessment of fluid dynamics using transthoracic echocardiography. Circulation 116:II_741.

Lisauskas, J. B., J. Singh, A. W. Bowman, and S. J. Kovács Jr. 2001a. Chamber properties from transmitral flow: prediction of average and passive left ventricular diastolic stiffness. J. Appl. Physiol. 91:154–162.

Lisauskas, J. B., J. Singh, M. R. Courtois, and S. J. Kovács Jr. 2001b. The relation of the peak Doppler E-wave to peak mitral annulus velocity ratio to diastolic function. Ultrasound Med. Biol. 27:499–507.

Mohseni, K., and M. Gharib. 1998. A model for universal time scale of vortex ring formation. Phys. Fluids 10:2436–2438.

Møller, J. E., E. Søndergaard, S. H. Poulsen, and K. Egstrup. 2000. Pseudonormal and restrictive filling patterns predict left ventricular dilation and cardiac death after a first myocardial infarction: a serial color *M*-mode doppler echocardiographic study. J. Am. Coll. Cardiol. 36:1841–1846.

Nagueh, S. F., K. J. Middleton, H. A. Kopelen, W. A. Zoghbi, and M. A. Quinones. 1997. Doppler tissue imaging: a non-invasive technique for evaluation of left ventricular relaxation and estimation of filling pressures. J. Am. Coll. Cardiol. 30:1527–1533.

Nagueh, S. F., C. P. Appleton, T. C. Gillebert, P. N. Marino, J. K. Oh, O. A. Smiseth, et al. 2009. Recommendations for the evaluation of left ventricular diastolic function by echocardiography. J. Am. Soc. Echocardiogr. 22:107–133.

Ommen, S. R., and R. A. Nishimura. 2003. A clinical approach to the assessment of left ventricular diastolic function by Doppler echocardiography: update 2003. Heart 89(Suppl. III):iii18–iii23.

Owan, T. E., D. O. Hodge, R. M. Herges, S. J. Jacobsen, V. L. Roger, and M. M. Redfield. 2006. Trends in prevalence and outcome of heart failure with preserved ejection fraction. N. Engl. J. Med. 355:251–259.

Park, H. S., S. D. Naik, W. S. Aronow, C. W. Ahn, J. A. McClung, and R. N. Blekin. 2007. Age- and sex-related differences in the tissue Doppler imaging parameters of the left ventricular diastolic dysfunction. Echocardiography 24:567–571.

Pasipoularides, A. 2010. Heart's vortex: intracardiac blood flow phenomena, 1st ed. People's Medical Publishing House, Shelton, CT.

Pedrizzetti, G., and F. Domenichini. 2005. Nature optimizes the swirling flow in the human left ventricle. Phys. Rev. Lett. 2005:108101-1–108101-4.

Riordan, M. M., and S. J. Kovács. 2006. Quantitation of mitral annular oscillations and longitudinal "ringing" of the left ventricle: a new window into longitudinal diastolic function. J. Appl. Physiol. 100:112–119.

Sadaniantz, A., B. J. Hadi, and L. S. Laurent. 1997. Gender differences in mitral inflow parameters of Doppler echocardiography. Echocardiography 14:435–439.

Schwartzenberg, S., M. M. Redfield, A. M. From, P. Sorajja, R. A. Nishimura, and B. A. Borlaug. 2012. Effects of vasodilation in heart failure with preserved or reduced ejection fraction. J. Am. Coll. Cardiol. 59:442–451.

Sengupta, P. P., G. Pedrizzetti, P. J. Kilner, A. Kheradvar, T. Ebbers, G. Tonti, et al. 2012. Emerging trends in CV flow visualization. JACC Cardiovasc. Imaging 5:305–316.

Shmuylovich, L., and S. J. Kovács. 2006. A load-independent index of diastolic filling: model-based derivation with in-vivo validation in control and diastolic dysfunction subjects. J. Appl. Physiol. 101:92–101.

Töger, J., M. Kanski, M. Carlsson, S. J. Kovács, G. Söderlind, H. Arheden, et al. 2012. Vortex ring formation in the left ventricle of the heart: analysis by 4D flow MRI and lagrangian coherent structures. Ann. Biomed. Eng. 40:2652–2662.

Zile, M. R., and D. L. Brutsaert. 2002. New concepts in diastolic dysfunction and diastolic heart failure: part I. Circulation 105:1387–1393.

Appendix A

The parametrized diastolic filling (PDF) formalism

A causal, kinematic, physiologic mechanism-based model of DF – the parametrized diastolic filling (PDF) formalism (Kovács et al. 1987) – has been previously derived and validated. The PDF formalism models suction-initiated filling in analogy to the motion of a damped, simple harmonic oscillator (SHO). Thus, PDF characterizes the Doppler *E*-wave as the solution to Newton's Law for SHO motion, using three parameters: k, chamber stiffness; c, chamber relaxation/viscoelasticity; and x_o, load. Most clinical *E*-waves are well fit by the "underdamped" ($c^2 < 4k$) regime with solution for the velocity:

$$E(t) = \frac{kx_o}{\omega} e^{-ct/2} \sin(\omega t) \text{ where } \omega = \frac{\sqrt{(4k - c^2)}}{2} \quad \text{(A1)}$$

The PDF parameters are calculated by using the *E*-wave contour as input. *E*-wave images are cropped, the maximum velocity envelope (MVE) is identified and used as input to fit the velocity of a damped oscillator using an iterative, error-minimizing Levenberg–Marquardt algorithm which has been described previously (Hall and Kovács 1994). The result solves the "inverse-problem of diastole" and provides unique PDF parameter values and the error of fit for each *E*-wave. The PDF parameters have invasive, gold-standard established physiologic analogues in terms of chamber stiffness, relaxation, and load (Kovács et al. 2000).

Appendix B

Equivalence of VFT standard expressions

The expression for $\text{VFT}_{\text{standard}}$ used in this work (eq. 1) is equivalent to equation (B1) which is the expression used by Gharib et al. (2006). In this appendix we demonstrate that our expression for $\text{VFT}_{\text{standard}}$ can be derived from Gharib's equation for VFT. The equation for VFT (which in Gharib et al. [2006] is referred to as T in eq. 1) is:

$$\text{VFT} = \frac{4(1-\beta)}{\pi}\alpha^3 . \text{ EF} \quad \text{where } \beta = \frac{V_A}{SV} \text{ and } \alpha^3 = \frac{\text{LVEDV}}{D_E^3} \quad \text{(B1)}$$

In the above equation, EF is ejection fraction, V_A is the volume of blood filling during the A-wave, SV is the stroke volume, LVEDV is the left ventricular end-diastolic volume, and D_E is the effective orifice diameter. VFT can be rewritten as:

$$\text{VFT} = \frac{4}{\pi}\left(1 - \frac{V_A}{\text{SV}}\right)\frac{\text{LVEDV}}{\text{D}_E^3} . \text{ EF} \Rightarrow \text{VFT}$$

$$= \frac{4}{\pi}\left(\frac{V_E}{\text{SV}}\right).\frac{\text{LVEDV}}{D_E^3}. \quad \text{(B2)}$$

Here, V_E is the *E*-wave volume. Given SV = EF·LVEDV and $\bar{U}_E = \bar{U}_E t\left(\frac{\pi \text{D}_E^2}{4}\right)$, where U_E is the mean *E*-wave velocity, t is the duration of *E*-wave (E_{dur}). Substituting the value of V_E and SV into the expression for VFT.

$$\text{VFT} = \frac{4}{\pi}\left(\bar{U}_E t \frac{\pi \text{D}_E^2}{4}\right)\frac{1}{\text{SV}}\frac{\text{SV}}{D_E^3} \Rightarrow \text{VFT} = \frac{\bar{U}_E t}{D_E} \quad \text{(B3)}$$

Hence, B1 and B3 are equivalent expressions and B3 is derived from B1. Assuming the *E*-wave shape as a triangle makes $\bar{U}_E t = \frac{1}{2}E_{\text{peak}} t$. Hence, we used B3 to calculate $\text{VFT}_{\text{standard}}$.